REPORT DOCUMENTATION PAGE

Form Approved
OMB No. 0704-0188

1. REPORT DATE *(DD-MM-YYYY)*
13-06-2007

2. REPORT TYPE
Technical Paper

3. DATES COVERED *(From - To)*

4. TITLE AND SUBTITLE

Dark Core Analysis of Coaxial Injectors at Sub-, Near-, and Supercritical Pressures in a Transverse Acoustic Field (Preprint)

5a. CONTRACT NUMBER

5b. GRANT NUMBER

5c. PROGRAM ELEMENT NUMBER

6. AUTHOR(S)
Ivett A. Leyva & Douglas Talley (AFRL/PRSA); Bruce Chehroudi (ERC)

5d. PROJECT NUMBER

5e. TASK NUMBER
23080533

5f. WORK UNIT NUMBER

7. PERFORMING ORGANIZATION NAME(S) AND ADDRESS(ES)

Air Force Research Laboratory (AFMC)
AFRL/PRSA
10 E. Saturn Blvd.
Edwards AFB CA 93524-7680

8. PERFORMING ORGANIZATION REPORT NUMBER

AFRL-PR-ED-TP-2007-327

9. SPONSORING / MONITORING AGENCY NAME(S) AND ADDRESS(ES)

Air Force Research Laboratory (AFMC)
AFRL/PRS
5 Pollux Drive
Edwards AFB CA 93524-7048

10. SPONSOR/MONITOR'S ACRONYM(S)

11. SPONSOR/MONITOR'S NUMBER(S)
AFRL-PR-ED-TP-2007-327

12. DISTRIBUTION / AVAILABILITY STATEMENT

Approved for public release; distribution unlimited (PA #07238A).

13. SUPPLEMENTARY NOTES
For presentation at the 43rd AIAA/ASME/SAE/ASEE Joint Propulsion Conference, Cincinnati, OH, 8-11 July 2007.

14. ABSTRACT
An experimental study on the effects of an externally-imposed transverse acoustic field in a N_2 shear coaxial jets at sub-, near-, and supercritical pressures is presented. Such fields and their interaction with the jets (i.e., breakup, mixing, etc.) are believed to play a critical role during combustion instabilities in liquid rocket engines. The shear coaxial injector used here is similar to those used in cryogenic liquid rockets. By using N_2 as the working fluid, the chemistry effects on combustion instability are separated from the effects of a transverse acoustic field on coaxial jets. Furthermore, through this choice, ambiguities associated with composition dependence on mixtures critical properties are eliminated. The acoustic field is generated by a piezo-siren and the first resonant frequency is ~3kHz. The pressures in the chamber range from 215-716 psia to span subcritical to supercritical pressures. The outer to inner jet velocity ratio varies from ~1.2 to 23 and the momentum flux ratio (MR) varies from ~0.2 to 23. These ratios are mainly varied by changing the temperature and flow rates of the outer jet. At least 2000 backlit images were taken at 41kHz for each run. The main metric investigated is the length of the dark, or inner jet, core. This length is related to the mixing processes in a coaxial jet. The shorter the core length the faster the mixing occurs. Both the axial and the total, or curved, dark core lengths are studied. For momentum flux ratios ~1<MR<~4 the differences in the axial and curved dark core lengths between acoustics on and off are statistically significant, which means acoustics do shorten the core for this range. For subcritical pressures the MR range where the jet is shortened is larger. Preliminary results on the frequency analysis of the dark core lengths and width is also presented.

15. SUBJECT TERMS

16. SECURITY CLASSIFICATION OF: a. REPORT	b. ABSTRACT	c. THIS PAGE	17. LIMITATION OF ABSTRACT	18. NUMBER OF PAGES	19a. NAME OF RESPONSIBLE PERSON / 19b. TELEPHONE NUMBER *(include area code)*
Unclassified	**Unclassified**	**Unclassified**	SAR	18	Dr. Douglas Talley / N/A

Standard Form 298 (Rev. 8-98)
Prescribed by ANSI Std. 239.18

Dark core analysis of coaxial injectors at sub-, near-, and supercritical pressures in a transverse acoustic field (Preprint)

Ivett A. Leyva[1], Bruce Chehroudi[2] and Douglas Talley[3]
Air Force Research Laboratory, Edwards AFB, CA 93524

An experimental study on the effects of an externally-imposed transverse acoustic field in a N_2 shear coaxial jets at sub-, near-, and supercritical pressures is presented. Such fields and their interaction with the jets (i.e., breakup, mixing, etc.) are believed to play a critical role during combustion instabilities in liquid rocket engines. The shear coaxial injector used here is similar to those used in cryogenic liquid rockets. By using N_2 as the working fluid, the chemistry effects on combustion instability are separated from the effects of a transverse acoustic field on coaxial jets. Furthermore, through this choice, ambiguities associated with composition dependence on mixtures critical properties are eliminated. The acoustic field is generated by a piezo-siren and the first resonant frequency is ~3kHz. The pressures in the chamber range from 215-716 psia to span subcritical to supercritical pressures. The outer to inner jet velocity ratio varies from ~1.2 to 23 and the momentum flux ratio (MR) varies from ~0.2 to 23. These ratios are mainly varied by changing the temperature and flow rates of the outer jet. At least 2000 backlit images were taken at 41kHz for each run. The main metric investigated is the length of the dark, or inner jet, core. This length is related to the mixing processes in a coaxial jet. The shorter the core length the faster the mixing occurs. Both the axial and the total, or curved, dark core lengths are studied. For momentum flux ratios ~1<MR<~4 the differences in the axial and curved dark core lengths between acoustics on and off are statistically significant, which means acoustics do shorten the core for this range. For subcritical pressures the MR range where the jet is shortened is larger. Preliminary results on the frequency analysis of the dark core lengths and width is also presented.

Nomenclature

A	=	constant
D	=	diameter with subscripts
LRE	=	liquid rocket engine
HE	=	heat exchanger
L	=	axial dark core length
Lt	=	total or curved dark core length
MR	=	outer to inner jet momentum flux ratio
n	=	exponent for *MR*
P	=	pressure
R	=	radius with subscripts
T	=	temperature
VR	=	outer to inner jet velocity ratio

Subscripts

i	=	inner-jet
o	=	outer-jet
cr	=	critical point

[1] Sr. Aerospace Engineer, AFRL/PRSA, Edwards AFB, CA 93524, AIAA Member.
[2] Principal Scientist, ERC Inc., AFRL, Edwards AFB, CA 93524, AIAA Member.
[3] Sr. Aerospace Engineer, AFRL/PRSA, Edwards AFB, CA 93524, AIAA Member.

I. Introduction

THIS study is conducted with two overarching objectives in mind. The first objective is to understand the effects of transitioning from subcritical to supercritical pressure on a coaxial injector's jet characteristics such as mixing, atomization and breakup. This is because as liquid rockets engines (LRE's) have evolved into higher specific impulse designs, the chamber pressures have simultaneously increased reaching supercritical for some propellants. The Space Shuttle Main Engine (SSME) and the Vulcan engine for the Ariane 5 launch vehicles are examples of LRE's designed to operate above the critical pressures of each propellant individually. We choose to study a coaxial injector since this design has proven effective for LRE's. In a typical coaxial injector for an LOX/LH2 engine, the oxygen is injected at subcritical temperatures in the center jet while the hydrogen is injected at supercritical temperatures, after being used as a coolant for the engine nozzle, in the coaxial jet. A typical velocity ratio between the outer and inner jets is about 10[1]. For these flows, as pointed out by previous researchers[1], the mixture no longer has a singular critical point but rather critical mixing lines that define its thermodynamic state. Therefore, a phase-diagram becomes necessary when studying mixtures that are at supercritical pressures with respect to their individual propellants. Because of the added complexity introduced when working with mixtures, we choose to first use N_2 as the sole working fluid.

The second objective is related to a problem that has been encountered since the late 1930's in LRE's, namely combustion instability[2]. Of the different types of instabilities, high frequency or acoustic instabilities are the most destructive to an engine. The damage can range from minor to catastrophic failure of an engine[3]. While a comprehensive understanding of what triggers these instabilities and how they evolve is still underway, a few things seem to be agreed upon. These instabilities are the result of coupling between the chamber acoustic modes and the injector fluid processes such as propellant injection, atomization, droplet vaporization, mixing and combustion heat release[4]. Of the different high-frequency acoustic modes, tangential modes (in the case of cylindrical chambers) seem to be the most damaging in rocket engines[5,6]. The equivalent of this mode in a rectangular chamber is a transverse mode. In the present study we have a coaxial jet with cryogenic N_2 in a rectangular chamber. We excite this jet with a piezo-siren that produces high amplitude (max ~ 184 db) pressure oscillations and sets up a transverse acoustic field. The second objective is then to study the effects of the acoustics on the jet. We do this mostly by measuring the jet's dark core length (indicative of mixing efficiency) and its standard deviation as we vary the outer-to-inner jet momentum flux ratio, MR, the outer-to-inner jet velocity ratio, VR, and the chamber pressure. By doing the experiments with cryogenic N_2, we aim to study the sub-process of acoustic interaction with the jet in isolation from the heat release created by the combustion process. In this sense, these cryogenic cold flow experiments at high pressure can be viewed as an intermediate step between atmospheric water cold flow experiments and fully reacting experiments. The data gathered in this study (with and without the imposed acoustic field) also serves as a first step validation for CFD codes aimed to tackle supercritical combustion.

A previous study done at the same facility at AFRL reported preliminary findings on the effects of a transverse acoustic field on a coaxial jet going from subcritical to supercritical pressures[7,8]. The current study is in part an extension of that work. The main differences are, 1) the ranges of MR and VR are larger in this study, 2) each data set now consists of at least 2000 images taken at a minimum sampling frequency of 41kHz (vs. 30 images taken at 10Hz), 3) introduction of the curved or total dark core length to look into a more detailed effects on mixing from the acoustics, 4) different definitions and smoothing techniques applied for computing the dark core length and are compared, and 5) a preliminary frequency analysis of the dark core length is given. With these enhancements, we have more confidence in the statistics of the dark core length and the conclusions drawn from these measurements.

II. Experimental Setup

The facility used for this study is the Cryogenic Supercritical Laboratory (EC-4) at the Air Force Research Laboratory (AFRL) at Edwards Air Force Base, CA. An overview of the facility is shown in Fig. 1. This facility has been extensively described in previous references [7, 8]. Gaseous N_2 is used to supply the inner and outer jet flows and to pressurize the chamber. It is obtained from the main supply line to the lab. The outer and inner jets are cooled by three heat exchangers (HE's). The coolant is liquid nitrogen obtained from a cryogenic tank. One heat exchanger cools the inner jet and the other two cool the outer jet. The temperature (T) of the two jets is controlled by adjusting the flow rate of liquid nitrogen through the HE's. The mass flow rate through the inner and outer jets is measured, before they are cooled, with Porter mass flow meters (122 and 123-DKASVDAA). It was found that it is much easier to measure the flow rates at ambient rather than at cryogenic temperatures. The chamber pressure is measured with a Stellar 1500 transducer. To keep the amplitude of the acoustic oscillations to a maximum near the jet, an inner chamber was created (Fig. 1). The inner chamber has nominal height of 2.6", width 3" and depth 0.5". Details for the coaxial injector used are shown in Fig. 2. The diameter of the inner jet is 0.020". The outer jet has an inner diameter, D2 of 0.063" and outer diameter, D3 of 0.095". The length to inside diameter is 100 for the inner jet and 67 for the outer jet (taking as reference the mean width of the annular passage, or hydraulic diameter). There is a small bias of about 8% of the mean gap width. As can be seen from the same figure, the inner jet is recessed by 0.010" from the outer jet.

The temperature of the jets is measured with a type E thermocouple which has a bead diameter of 0.004". The accuracy of this thermocouple was checked with an RTD and found to be 1K. This thermocouple is traversed across the outer and inner jets to obtain a reading as close as possible to the injector exit plane (also seen in Fig. 1). The radial profiles of the temperature were taken at intervals of 0.004" or 0.002" if the temperature varied significantly. The average distance from the exit plane, denoted H in Fig. 2 is ~0.012". Properties such as density, viscosity, and surface tension are computed from the measured flow rates, chamber pressure and jet temperature, using NIST's REFPROP[9]. From this, the Re, We, VR and MR for a given condition can be computed.

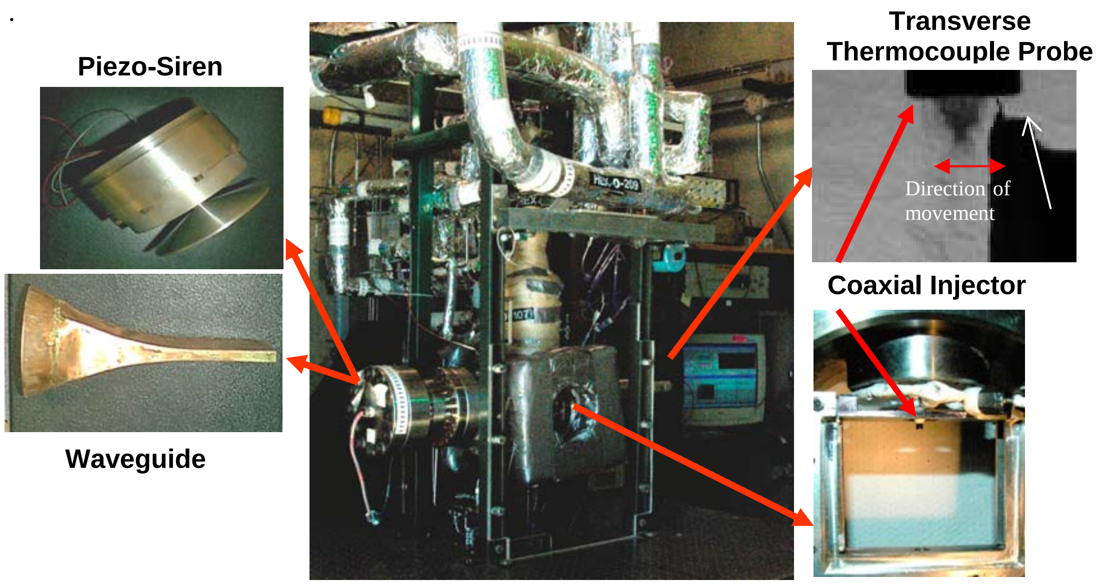

Figure 1. Overview of the Supercritical Flow Facility, EC-4 at AFRL/Edwards used for this study

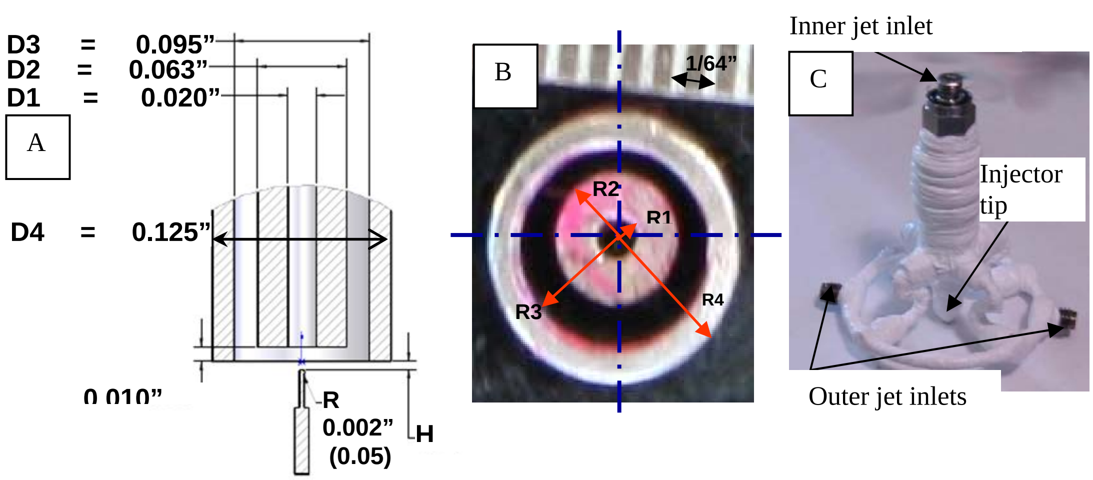

Figure 2. Details on the coaxial injector used for the present study

The jet is visualized by taking backlit images using a Phantom 7.1 CMOS camera. The images have 128x256 pixels, and each pixel represents an area of about 0.003”x0.003”. The framing rate was 41kHz. The exposure time varies from 7-9μs. The jet is backlit using a Newport variable power arc lamp set at 300W. The acoustic waves are generated using a piezo-siren custom-designed for AFRL by Hersh Acoustical Engineering, Inc. (Fig.1). A piezo-ceramic element is externally excited with a sinusoidal wave at the desired driving frequency for the system. This frequency is chosen by manually varying the frequency on a signal generator until the highest amplitudes for the pressure waves are obtained. This signal is amplified and then fed to the piezo-siren. The movement of the piezo element is transmitted to the aluminum cone attached to it, and the cone then produces acoustics waves. To accommodate for the rectangular chamber a waveguide with a catenary contour is used to guide the waves from a circular cross-section to a rectangular cross-section (also shown in Fig.1). The sound pressure levels (SPL) in the inner chamber range from 161 dB to 171 dB at for the first two resonance frequencies (~3.0 kHz and ~5.2 kHz). In this study only the first resonant frequency is studied.

IV. Results and Discussion

A total of 44 runs were completed spanning chamber pressures from 215 to 716 psia. The runs are divided into subcritical, nearcritical and supercritical pressures. Details of the test run conditions are presented in the Appendix. Table 1 summarizes the range of conditions for each chamber pressure. Since the major parameter of interest for this study is the core length, a graphical representation of the definitions for the axial and curved or total length is shown in Fig. 3.

Table 1. Summary of range of conditions for each pressure range
.

Mean Chamber pressure, P (psia)	Outer to inner jet Velocity ratio, VR	Outer to inner jet momentum flux ratio, MR	Range of inner jet temperature (F)	Nominal inner jet mass flow rate (lb/s) x10-6	Range of outer jet temperature (F)
215	1.9-22.5	0.2-23.2	-262	617	-200 – -109
515	1.3-5.3	0.3-6.6	-235 to -227	637	-211 – -109
716	1.2-4.8	0.4-10.3	-222 to -211	648	-190 – -109

As a reference, in this figure, Pchamber =217 psia, VR=7.50, MR=2.64 and the acoustic field is on. Our first observation in the unprocessed image (leftmost image) is that the inner jet, which is colder and denser than the outer jet, shows darker in the backlit image. It is the length of this denser core, before its first break, that is called the dark core length. Historically, people have defined the dark core length or intact length as the projection of the core in the axial direction as shown in Fig. 3. In this study, this is called the axial dark core length. There are many valid ways to define this length. One only has to be cautious that the method chosen agrees with the intuitive length judged by the naked eye. Several methods to compute the axial dark core length were analyzed by this group. In general, to arrive to a length from raw images, a series of steps need to be taken. The first step is to convert the grayscale images to black and white (b&w) images. This is typically done by choosing a threshold value of pixel intensity below which all pixels are set to black and above which all pixels is set to white. Choosing an adequate threshold is the first logic rule that is implemented when automating the length measurement. After converting the image to b&w one has to define the first break in the jet. This would be the second logic rule that is implemented. Finally, if a total or curved length is desired (Fig 3), then one needs to decide if the curve needs to be smoothed before the final curve measurement is made.

In the present case, the raw images taken with the Phantom camera are first converted to a multi-page tiff format and then analyzed using Matlab. Matlab was chosen over other image processing programs such as ImagePro because it is faster. The raw images are converted, or thresholded, to a b&w image using Matlab’s subroutine “im2bw” (Fig. 3B). The threshold level is determined using matlab subroutine “graythresh”. This subroutine uses

Otsu's method[10] and it is based on the zeroth and first cumulative moments of the gray-level histogram. In previous studies from this group[7-8] the threshold was found by constructing a histogram of the image and defining the threshold value as the pixel intensity where the slope of histogram is equal to 1/e. The current method to define a threshold is preferred due to its robustness. Once a b&w image is obtained, the axial length of the jet is determined by drawing a contour around the image (using matlab subroutine "imcontour") and measuring the y coordinate of the longest contour that is attached to the injector as shown in Fig. 3. Other ways to define the length include measuring the location when the standard deviation of the pixel intensity of a row is zero. This method tends to ovepredict the length when the jet break is not clean and there are dark lumps clustered around the jet breakup region. For clean breaks both methods agree very well. It is noteworthy to say that even though the magnitudes might be different with the different definitions for the lengths, the trends of the axial dark core length and its standard deviation with respect to MR and VR are preserved.

In an attempt to investigate whether the transverse acoustic field shortens the length of the jet or if it only bends, a curved or total length was also measured. In this case, the same contour already used to measure the axial length is divided into a left and a right side (see Figure3C). The total length is defined as the average of the left and right sides. Because the curves had a lot of small scale spatial features believed not to be significant to the computation of the total length, the right and left sides were smoothed by three methods: 1) simple averages in the x and y direction (5 points), 2) median filtering, and 3) median filtering followed by simple averages. The simple average was chosen because it smoothed out the small scale features mentioned above while preserving the shapes of the larger scale structures which is what we are interested. Similarly in the case of filtering, even though the magnitude of the curved length changes, the trends with respect to MR and VR are preserved.

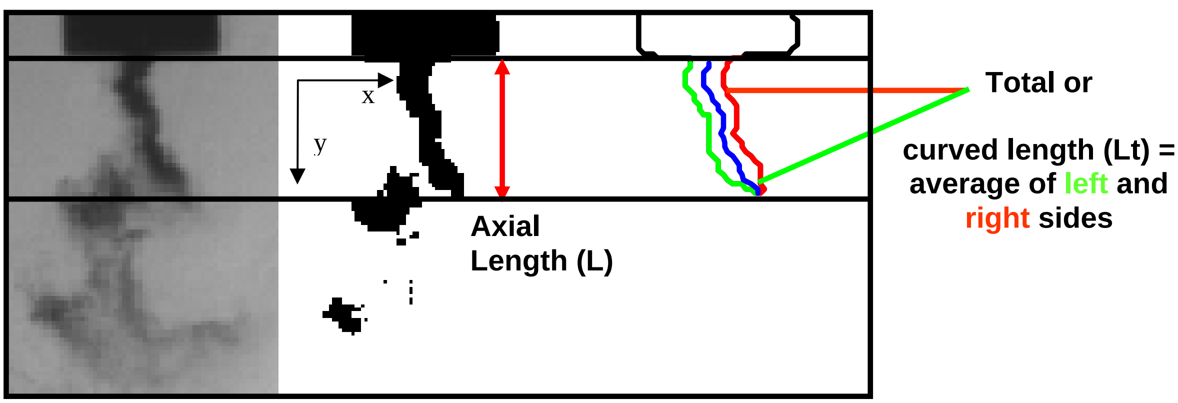

Figure 3. A. Raw image. B. Black and white image after thresholding showing definition of axial dark core length. C. Definition of total or curved length.

The lengths given by the matlab subroutines were manually checked by selecting 50-60 images from each set of 2000 images and comparing the results with what the authors would select to be the length using the naked eye. Using these images the threshold level could be modified, if needed, from the one automatically computed and then used to process the complete set of images.

A. Qualitative Characterization of Images

A collection of the images taken at the three different chamber pressures are shown in Figs. 4-6. The first set of images (Fig. 4) corresponds to a subcritical pressure. For this case, the inner jet is a liquid with a saturation temperature of 109-110K and the outer jet is a gas with temperature from 170-200K. This is a two-phase mixture. The upper row of images has the acoustic field turned off. In the leftmost image the presence of droplets is evident, but as the VR and MR increase the dark core and the droplets become smaller and finally, for the conditions of the rightmost image, the droplets have become irresolvable by the pixel size of the image. This behavior is consistent with previous data[7-8] where as MR and VR increase the mixing becomes more efficient between the two jets and the inner jet mixes faster with its surroundings. When the transverse acoustics field is turned on (lower row in Fig. 4), we can see the jet moving in the transverse direction as well. As we will show later, the movement of the jet has the same frequency as the driving frequency of the piezo-siren. We can also intuitively see that the acoustics have the most effect on the jet, in terms of the decrease in axial dark core length and the amount of discernable bends, in a range of MR from about 1-4, which we will also confirm quantitatively later.

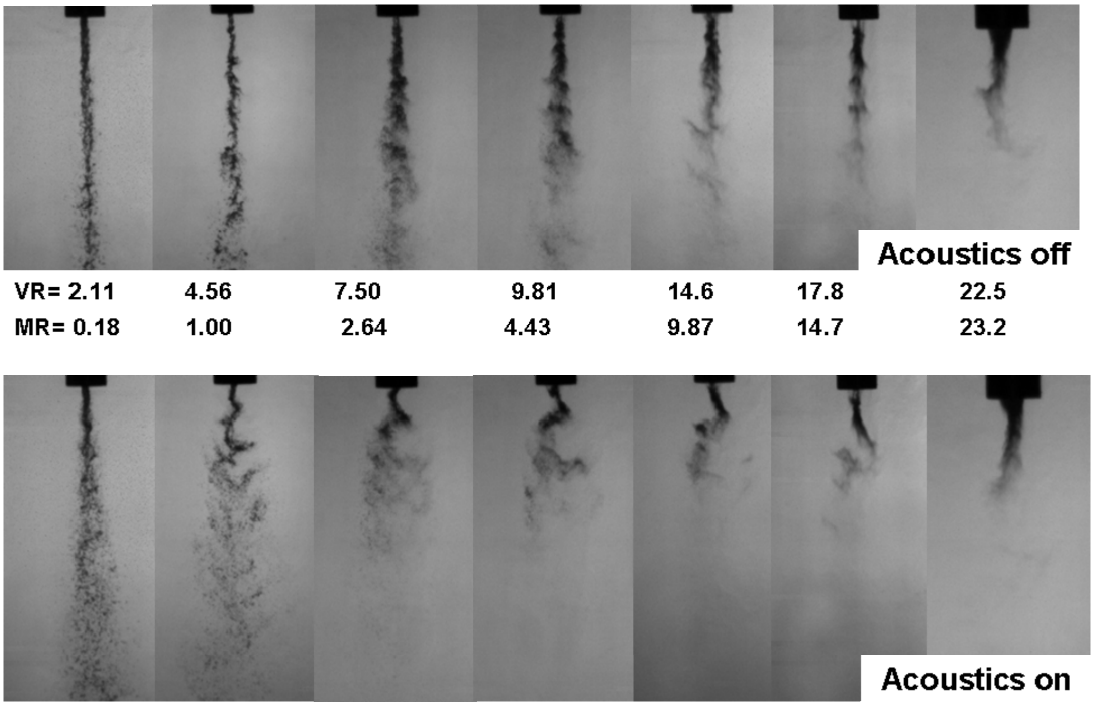

Figure 4. Collection of images at subcritical pressure (~215 psia) with acoustics on and off for MR:0.18-23.2 and VR:2.11-22.5. The driving frequency is ~3kHz.

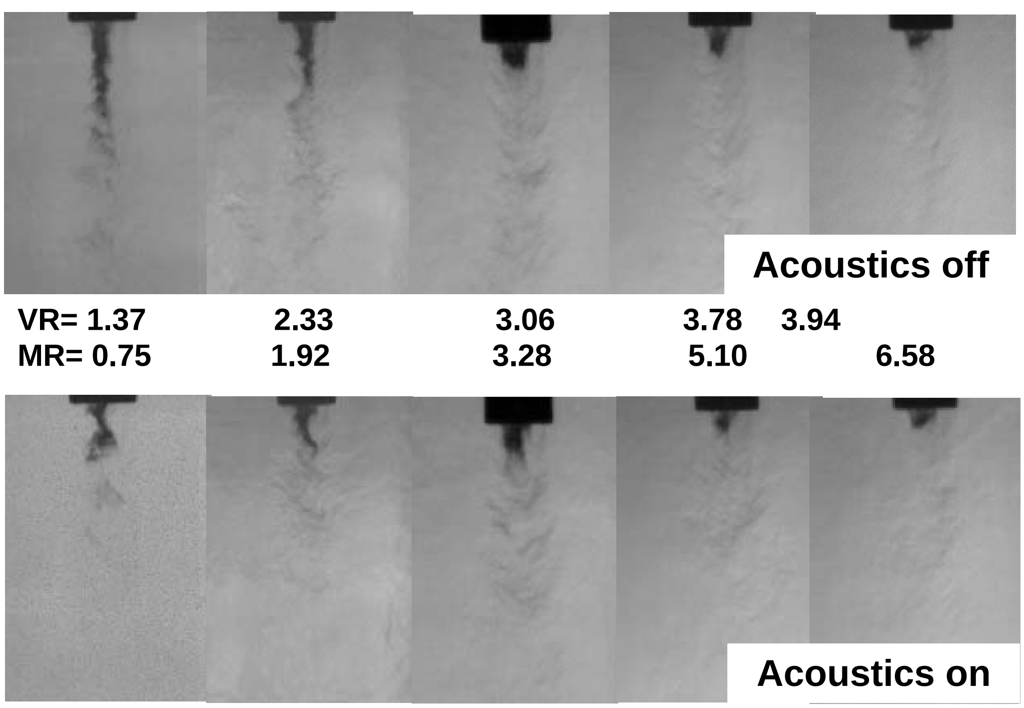

Figure 5. Collection of images at nearcritical pressures (~515 psia) for acoustics on and off for MR:0.75-6.58 and VR:1.37-3.94

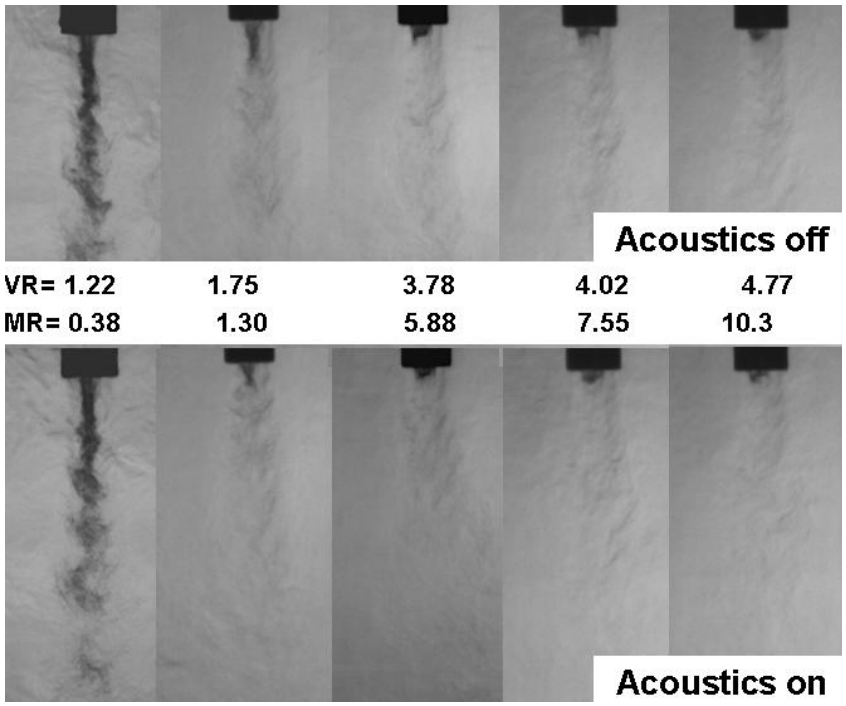

Figure 6. Collection of coaxial jet at supercritical pressure (~716psia) with acoustics on and off for MR: 0.38-10.3 and VR: 1.22-4.77. The driving frequency is ~3 kHz

traveling in the transverse direction as well. As we will show later, the movement of the jet has the same frequency as the driving frequency of the piezo-siren used to establish the imposed external acoustic field. We can also intuitively see that the acoustics have the most effect on the jet, in terms of the decrease in axial dark core length and the amount of discernable bends, in a range of MR from about 1 to 4, which we will also confirm quantitatively later.

As we move to nearcritical conditions (Fig. 5) we notice some differences. In this case the inner jet is a few degrees above the critical temperature and the outer jet temperature varies from 170-200K. Both jets are in a supercritical state. This is a one-phase mixture. Notice that there are no more visible droplets in this situation, even for the low VR's, as we would expect since the inner jet is not a liquid anymore. At this pressure, the dark core length has become smaller for a given MR and VR and, by VR values of ~4, the length of the jet has become equal to 1 to 2 times D1. In this case, when the acoustics are turned on, we still see a dramatic shrinkage in the axial length for the 2 leftmost images, but as the MR increases the changes become less discernable and the bending of the jet becomes more of a straight motion of the short jets in the transverse direction. Similar observations apply for Fig. 6 which depicts jets at supercritical pressures and supercritical temperatures as well.

B. Axial Dark Core Length

From the qualitative visualizations, we move on to quantitative characterization of the jet's response to the acoustic field by plotting the axial dark core length as a function of MR. The results are shown in Fig. 7. This figure includes all data gathered in this study only. Solid symbols correspond to data with no acoustics and the hollow symbols correspond to data when the acoustics are on. The color codes and symbols are applicable also to the rest of the figures in this paper. The error bars denote $\pm 1\sigma$ (standard deviation). The two sets of blue data correspond to subcritical pressures. Within subcritical pressure data, the light blue or cyan corresponds to a set of data taken with a nearly constant outer jet temperature of 180-181K. This was done to compare with other data set to see if there was a direct effect of the outer jet temperature (besides its implicit effect through density and MR) on the dark core length. As the figure shows, these data blend well with the rest of the subcritical data which includes a broad range of outer jet temperatures from 130K to 210K. Therefore, there is no direct effect of the outer jet temperature on the axial dark core length within the range of MRs tested here. The other point to indicate has to do with the system repeatability in the subcritical regime. For a few conditions (namely around MR=1 and MR=5), data were repeated within with a few weeks to a couple of months. In all cases the variability is within the error bars of the test data.

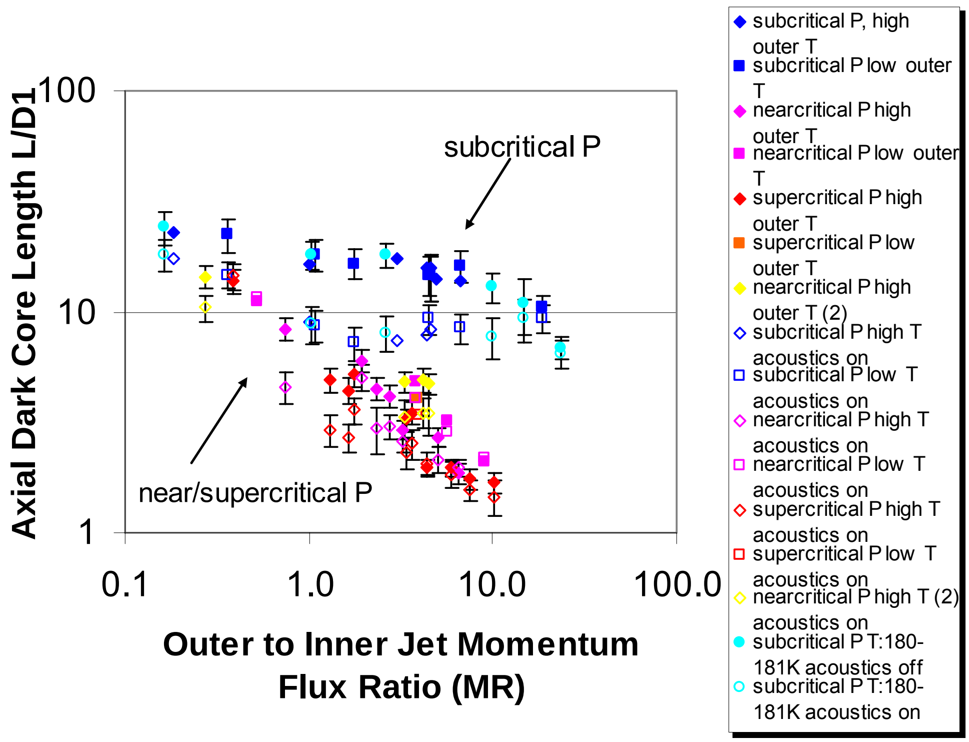

Figure 7. Variation of the Axial Dark Core Length as a function of MR for both acoustics on and off

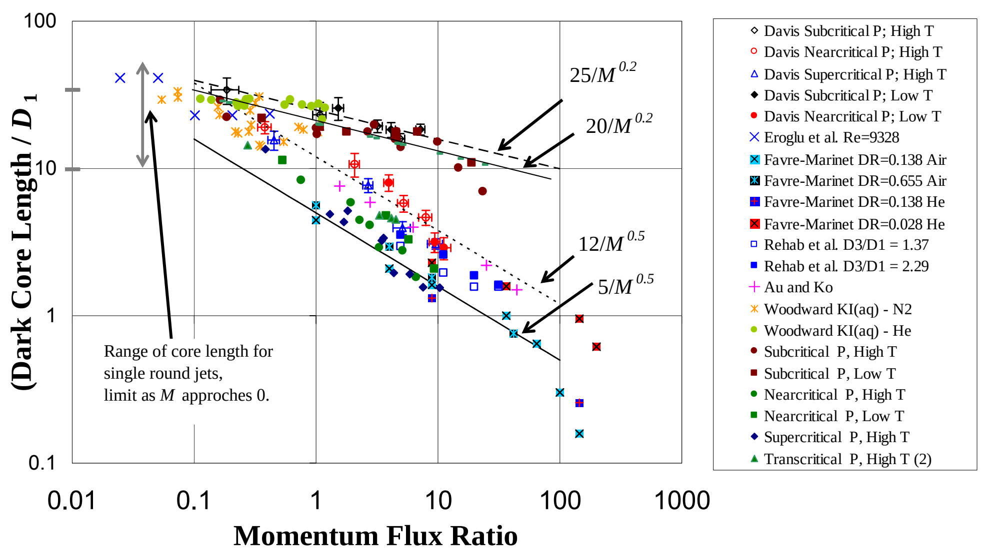

Figure 8. Summary of historical and current data on the trends of the axial dark core length vs. MR

The magenta data is for nearcritical pressures with the inner jet at supercritical temperatures. The yellow data points are also at nearcritical pressures but the temperature of the inner jet is within 1K of the critical temperature. Finally the red data corresponds to supercritical pressures. One of the most striking things from this figure is that there are indeed two branches for the dark core length plotted versus the MR. This new data confirms previous data gathered in this facility other historical data [7,8]. In fact this was one of the objectives of the present study, namely to verify the trends of the axial dark core length vs. MR with more robust statistics due to the fact that we have more data points per run than before. Also, note that differences in the axial dark core length for acoustics on and off cases are statistically significant for ~1<MR<~4 under all chamber pressures. This is especially clear for the subcritical pressures. Next, this data is plotted along with the previously gathered data from this facility[8] and the historical data by others (Fig. 8). In previous studies[7,8] the trend for the single-phase mixtures (near and supercritical P) was shown to follow a functional relation of the form A/MR^n where n is 0.5 and A:[5-12] whereas for the two-phase mixtures (subcritical P) the exponent was 0.2 and A was 25. With the exception of the constant A being 20-25 for the subcritical P, the data from this work is also captured by the same functional relations.

A trend that wanted to be verified with this study is the effect of VR on the standard deviation (std. dev.) of the axial dark core length. This is because preliminary data [7,8] indicated that the std. dev. decreased with VR offering perhaps insight into why injectors for cryogenic liquid rocket engines designed for high VR are in practice provide a more stable combustion than those working at lower VR's. That is, a lower std. dev. is indicative of the jet's insensitivity to externally imposed acoustics which would make it more "stable". Of course, this and the previous studies are performed with N_2 instead of combusting gases, and this hypothesis needs to be tested with fired engines. The results for the axial length std. dev. are presented in Fig. 9 for all the data gathered in this study. The general trend, with the exception of a few outliers, is the same as observed before. The std. dev. decreases with VR, especially for the near and supercritical pressures. A new observation that can be made from this data set, which contains more data points that previous data sets [7, 8], is the fact that the fastest drop in std. dev. values happens at low VR's. At around VR=5, the std. dev. decrease is more gentle. Also, note that the std. dev.'s of the cases with acoustics on are lower than their no-acoustics counterparts and follow the same trend. For the near and supercritical pressure cases, when the lengths become small enough (<0.5D1) no conclusions can be drawn as the pixel resolution for these images is ~0.2D1.

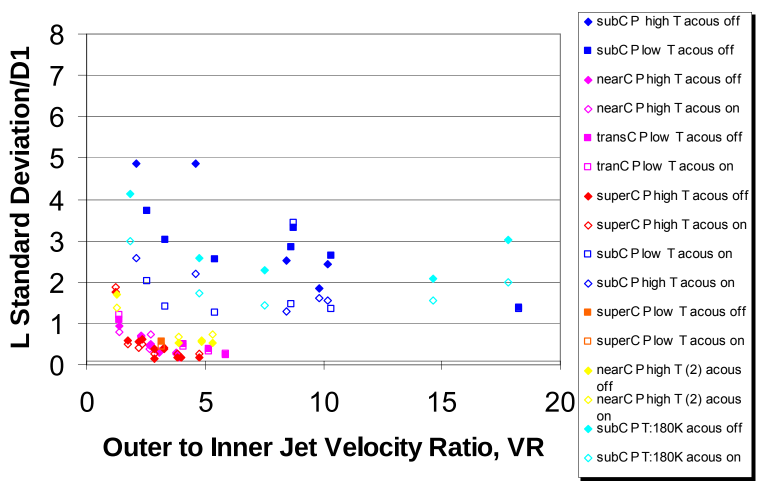

Figure 9. Standard deviation of the axial dark core length vs. VR

C. Curved or Total Dark Core Length

One of the questions that arose while conducting this study was whether the acoustics were indeed shortening the dark core or merely bending it. If the core is only being bent then we would expect the acoustics not to have much effect on mixing but if the core is being bent and shortened then acoustics is expected to have a more enhanced impact on mixing. To answer this question, the definition of curved length described in Fig. 3 was employed. As mentioned previously, the curved lengths were smoothed by using a 5 point average around every point both in the x and y directions. Fig. 10 shows the results for the curved dark core length vs. MR. This figure is the counterpart to Fig. 7. One interesting observation is the great resemblance between both figures. In fact, except for the fact that the lengths are larger (as intuitively expected) all the observations made for Fig. 7 still apply. However, by virtue of Fig. 10 having curved as compared to axial lengths, the fact that we see statistically significant differences between the cases with and without acoustics means that the jet is indeed shortened by the acoustic field when ~1<MR<~4. These differences are clearer in the curved dark core lengths. Finally, to conclude the comparison between the curved and axial dark core lengths, the std. dev. has been plotted against VR in Fig. 11. The data shows more scatter than those for the axial dark core length but the general trends are the same.

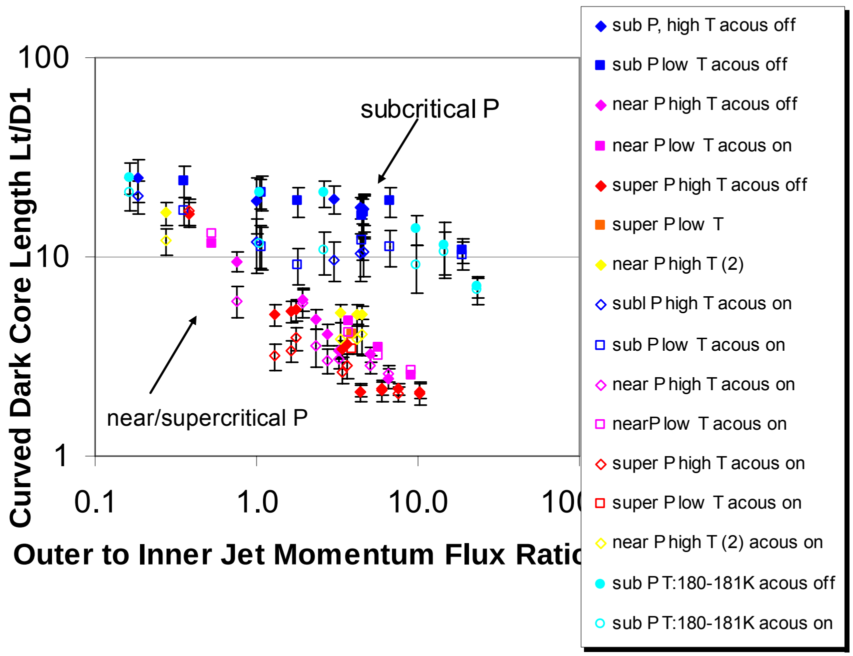

Figure 10. Trend of the Curved Dark Core Length vs. MR

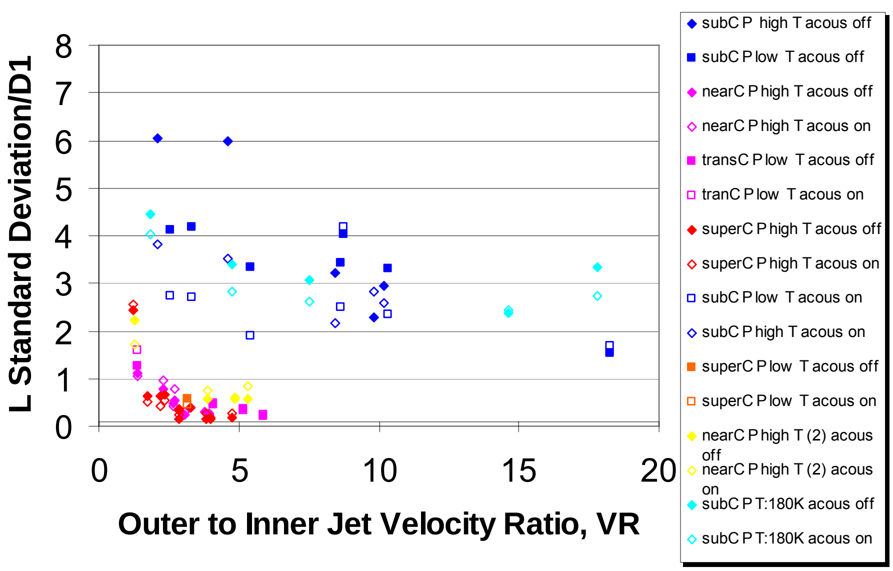

Figure 11. Standard Deviation of the Curved Dark Core Length vs. VR

D. Frequency analysis

The last part of this paper is a preliminary presentation of the frequency analysis done on the transverse and axial movements of the dark core of the jet. Fig. 12 A&B shows a sample of the axial and curved lengths as a function of time for Run #** for when the acoustics were on. In both cases, the dominant frequency is so prevalent that one can estimate it by merely counting the peaks. Also, note that the lengths have a saw tooth shape vs. the sinusoidal shape of the signal that is fed into the piezo-siren. Fig. 13 A&B shows the FFT's of the axial and smooth curved lengths. The fundamental frequency in both cases is also about 3.023 kHz vs 3.04 kHz fed into the piezo-siren, which is a very good agreement. The FFT of the right side, left side, and width of the dark core is shown in Fig. 14 A-C. For every row in the image where there is an attached dark core, the right side is defined as the difference between the x-coordinate of the right side of the contour (Fig. 3) and the geometric center of the inner jet. Similarly, the left side is defined as the difference between the x-coordinate of the left side of the jet contour (Fig. 3) and the geometric center of the injector. In this case, these FFT's are for the 3rd row after the injector exit plane. We see that the main frequency is again 3.023kHz. Together, the left and the right sides as well as the width tell the story of the dynamics of the jet. Because the left and right edges of the core are moving, the peak in the width is attributed not to a stationary pulsing of the width but to the fact that the entire width is traveling to the left and right and contracting and expanding in the process. These preliminary results hint to the complex motion of the dark core of the jet in the transverse and axial directions when affected by a transverse acoustic field. A more detailed study of the frequency analysis of the behavior of the jet will be the subject of future papers.

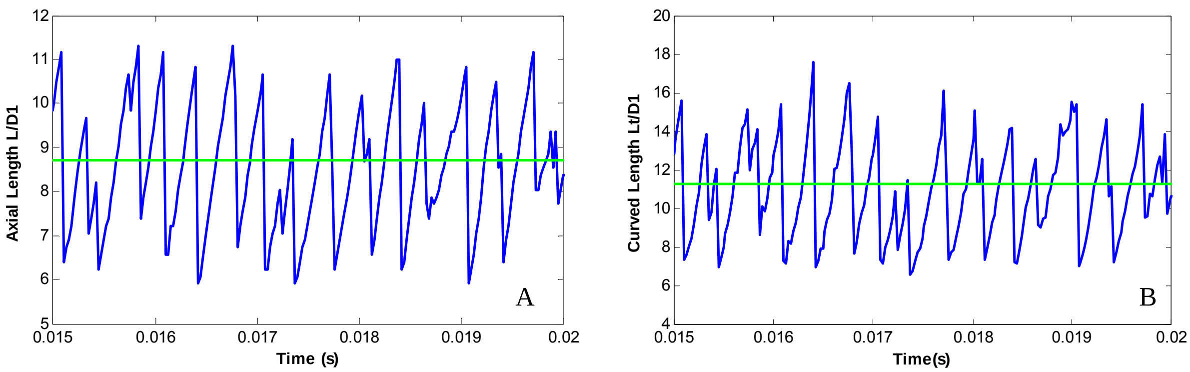

Figure 12. A. Time trace of axial dark core length. B. Time trace of curved dark core length.

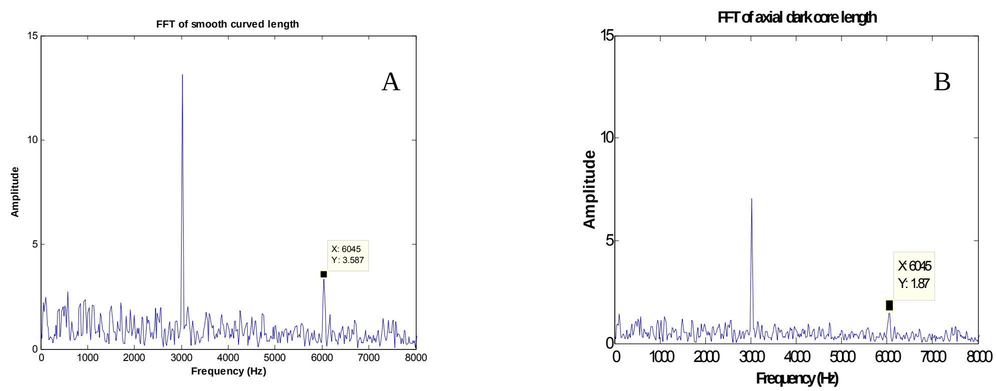

Figure 13. A. FFT of axial dark core length. B. FFT of curved dark core length

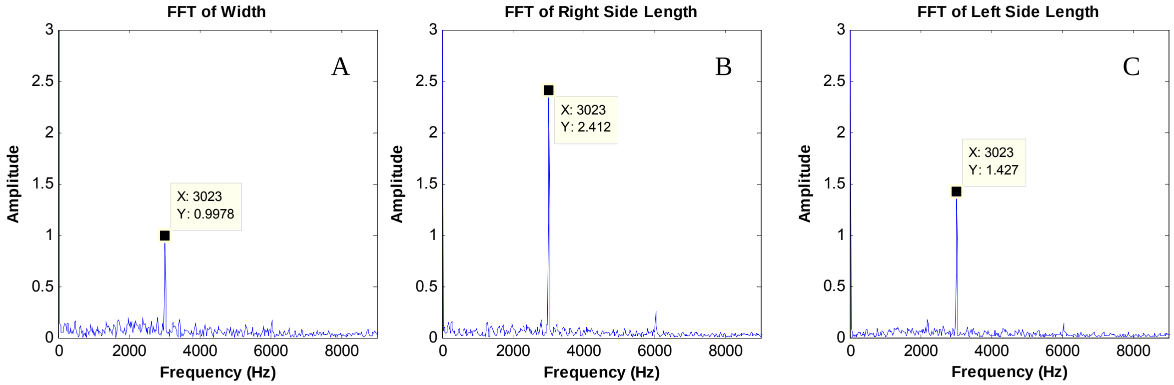

Figure 14. A. FFT of width of dark core. B. FFT of Right Side Edge. C. FFT of Left Side Edge

V. Conclusion

An extensive study was carried out to characterize the effects of a transverse acoustic field on a coaxial jet spanning subcritical to supercritical chamber pressures. The main metric used to assess the effects of the acoustics and operating conditions on the jet is the dark core length. Both an axial and a total or curved length were defined. In this study, at least 2000 frames were obtained for each run condition such that the mean and the standard deviation of the dark core length are more robust than those gathered in a previous study which consisted of 30 frames per condition. With the new data set, conclusions reached before are mostly confirmed, and in addition new opportunities were offered for a more detailed analysis of the jet dynamics. The decrease of the standard deviation of the dark core length (both axial and curved) with VR is confirmed. As the standard deviation decreases the jet becomes more insensitive to external fluctuations which can offer insight into why liquid rocket engine injectors designed to operate at VR>~10 s are more stable that those designed to operate at lower VR values. The current axial dark core length data also falls within a band defined by $L=A/MR^n$, with the exponent being 0.2 (A:20-25) for subcritical pressures, and 0.5 (A:5-12) for near and supercritical pressures. With the exception of opening the band from A=20 to A:20-25 for subcritical pressures, the results agree with previous data.

A new key finding, however, is that for ~1<MR<~4, acoustics do shorten the dark core which implies that acoustics enhance mixing in this range. This answers the question of whether the acoustic field imposed on the jet only bends the jet or bends it and shortens it. For this range of MR's the differences in the curved lengths are larger than the error bars ($\pm\sigma$) in the data. This range is even larger for subcritical pressures. Outside this range the differences between the curved dark core length with and without acoustics fall within the statistical uncertainty of the measurements. Especially for MR>~4 in the near and supercritical pressures, the core becomes so small (1-2 D1) that the differences between acoustics on and off fall within the resolution of the camera. This implies that acoustics do affect mixing for this range. Preliminary data is also presented to characterize the frequencies of the jet's movement in the transverse and axial directions. As one would expect, the frequency describing the transverse and axial movements of the jet is the same as the driving frequency of the acoustic field. Future work will include further characterization of the acoustic pressure field which will give us a precise measurement of the acoustic pressure field for every condition. Also, further frequency analysis of the jet, and variation of the position of the pressure and velocity nodes with respect to the jet center will be performed. This last part will allow us to see the effects not only of magnitude but also of gradient of the acoustic pressure and velocity on the jet's behavior.

Appendix

	SUBCRITICAL PRESSURE										
	HIGH OUTER JET TEMPERATURE										
	sb1	sb2	sb3	sb4	sb5	sb6	sb7	sb8	sb9	sb10	sb11
T chamber (K)	231	237	252	240	243	241	250	243	245	250	214
ρ chamber (kg/m^3)	22.4	21.1	19.9	21.1	21.0	20.8	20.3	20.9	20.6	20.1	24.0
P chamber (MPa)	1.51	1.46	1.47	1.49	1.49	1.47	1.49	1.49	1.48	1.48	1.49
P chamber (psia)	220	212	213	216	217	213	216	216	214	214	216
T outer (K)	181	195	175	180	181	195	184	189	181	181	184
$\dot{m}$ outer (mg/s)	316	315	785	787	1270	1260	1620	1600	2410	2950	3680
ρ outer (kg/m^3)	29.6	26.2	29.8	29.2	29.2	26.4	28.6	27.5	28.8	28.8	28.5
u outer (m/s)	4.09	4.61	10.1	10.3	16.6	18.3	21.6	22.2	32.1	39.1	49.4
Re outer	4.14	3.89	10.5	10.3	16.6	15.6	20.9	20.2	31.6	38.6	47.7
T inner (K)	110	109	110	109	110	110	110	110	110	110	110
$\dot{m}$ inner (mg/s)	281	281	280	280	282	278	280	278	279	280	279
ρ inner (kg/m^3)	625	629	626	629	621	625	621	624	623	623	626
u inner (m/s)	2.21	2.21	2.21	2.20	2.24	2.19	2.22	2.20	2.21	2.22	2.20
Re inner	12.4	12.3	12.4	12.2	12.7	12.3	12.6	12.4	12.5	12.6	12.4
VR	1.86	2.11	4.60	4.73	7.49	8.43	9.81	10.2	14.6	17.8	22.6
MR	0.164	0.185	1.01	1.04	2.64	3.00	4.43	4.59	9.87	14.6	23.3
Acoustics Off											
L/d1	24.0	22.7	16.5	18.1	18.2	17.5	15.9	15.7	12.9	10.9	6.89
L_T/d1	25.1	24.8	19.0	20.9	20.9	19.6	17.7	17.4	13.8	11.5	7.06
Acoustics On											
Frequency (kHz)	2.97	2.95	2.99	2.97	2.97	2.97	2.99	2.97	2.97	3.00	3.03
L/d1	18.2	17.4	8.90	8.79	8.05	7.47	7.86	8.28	7.71	9.31	6.43
L_T/d1	21.0	20.1	11.8	11.7	10.8	9.65	10.3	10.6	9.03	10.5	6.77

	SUBCRITICAL PRESSURE							NEARCRITICAL PRESSURE			
	LOW OUTER JET TEMPERATURE										
	sb12	sb13	sb14	sb15	sb16	sb17	sb18	nr12	nr13	nr14	nr15
T chamber (K)	233	221	228	234	213	213	213	216	210	215	209
ρ chamber (kg/m^3)	21.5	23.3	22.1	21.5	23.9	24.2	24.1	58.7	60.3	58.7	60.5
P chamber (MPa)	1.46	1.49	1.48	1.47	1.47	1.50	1.48	3.57	3.54	3.54	3.54
P chamber (psia)	212	217	214	213	214	217	215	517	513	514	513
T outer (K)	157	112	146	148	148	144	154	138	143	157	141
$\dot{m}$ outer (mg/s)	504	1170	1170	1860	1860	2320	3690	1410	3450	4040	5650
ρ outer (kg/m^3)	33.9	61.0	37.8	37.1	37.1	39.1	35.2	130	115	94.3	121
u outer (m/s)	5.69	7.36	11.9	19.1	19.2	22.7	40.1	4.14	11.5	16.4	17.8
Re outer	7.36	21.7	18.1	28.5	28.5	36.3	54.6	19.1	47.0	53.6	77.0
T inner (K)	109	110	110	110	110	110	110	125	123	126	125
$\dot{m}$ inner (mg/s)	284	281	279	281	279	278	280	291	292	286	287
ρ inner (kg/m^3)	628	619	625	623	621	619	624	482	508	442	465
u inner (m/s)	2.23	2.24	2.20	2.23	2.21	2.22	2.21	2.98	2.84	3.19	3.05
Re inner	12.4	12.8	12.4	12.6	12.6	12.7	12.5	22.0	20.2	24.9	23.1
VR	2.58	3.31	5.43	8.66	8.74	10.3	18.3	1.40	4.09	5.17	5.89
MR	0.358	1.08	1.78	4.47	4.55	6.73	18.8	0.530	3.77	5.72	9.06
Acoustics Off											
L/d1	22.3	18.2	16.5	14.7	14.5	16.1	10.4	11.1	4.85	3.23	2.09
L_T/d1	24.1	21.2	19.1	16.0	16.6	19.0	10.9	11.7	4.80	3.50	2.52
Acoustics On											
Frequency (kHz)	2.96	3.04	3.06	3.07	3.05	3.04	3.02	3.12	3.11	3.13	3.13
L/d1	14.7	8.72	7.21	9.32	14.5	8.43	9.37	11.6	4.09	2.85	2.18
L_T/d1	17.1	11.3	9.17	12.1	16.6	11.2	10.2	13.0	4.19	3.22	2.68

	NEARCRITICAL PRESSURE – HIGH OUTER JET TEMPERATURE										
	ABOVE CRITICAL INNER JET TEMPERATURE							BELOW CRITICAL INNNER JET TEMPERATURE			
	nr1	nr2	nr3	nr4	nr5	nr6	nr7	nr8	nr9	nr10	nr11
T chamber (K)	254	228		251	234	247	238	237	232	236	230
ρ chamber (kg/m^3)	47.6	54.8		48.8	53.1	49.8	51.9				
P chamber (MPa)	3.52	3.56	3.58	3.54	3.56	3.55	3.54	3.53	3.56	3.55	3.56
P chamber (psia)	510	517	518	514	516	515	514	511	517	515	516
T outer (K)	194	179	179	186	171	192	195	182	189	184	194
$\dot{m}$ outer (mg/s)	2030	3070	3130	3850	3950	4950	6120	802	3140	3140	3130
ρ outer (kg/m^3)	66.4	75.5	75.9	70.9	80.8	68.0	66.7	72.9	69.7	72.6	67.2
u outer (m/s)	11.7	15.5	15.8	20.8	18.7	27.9	35.1				
Re outer	23.8	37.9	38.7	46.4	50.1	58.5	71.8				
T inner (K)	130	128	128	129	128	129	132	126	127	127	126
$\dot{m}$ inner (mg/s)	289	290	289	290	288	287	286	287	288	288	288
ρ inner (kg/m^3)	167	213	244	182	230	190	157	422	319	416	420
u inner (m/s)	8.56	6.72	5.84	7.88	6.18	7.44	8.97				
Re inner	58.2	52.1	47.5	56.4	49.4	54.6	58.5				
VR	1.37	2.33	2.72	2.66	3.05	3.77	3.94	1.26	3.89	4.88	5.32
MR	0.751	1.93	2.31	2.76	3.27	5.09	6.59	0.28	3.31	4.15	4.52
Acoustics Off											
L/d1	8.39	6.00	4.47	4.17	2.94	2.71	1.85	14.7	4.80	4.89	4.69
L_T/d1	9.48	6.14	4.86	4.07	3.35	3.23	2.47	16.6	5.23	5.17	5.10
Acoustics On											
Frequency (kHz)	3.00	2.99	3.05	3.05	3.01	3.06	3.05	3.06	3.01	3.02	3.00
L/d1	4.57	5.06	2.99	3.00	2.60	2.15	1.97	10.4	3.33	3.49	3.50
L_T/d1	6.00	5.91	3.57	3.01	3.05	2.87	2.58	12.0	3.88	3.88	4.06

	SUPERCRITICAL PRESSURE										
	HIGH OUTER JET TEMPERATURE										LOW T
	sp1	sp2	sp3	sp4	sp5	sp6	sp7	sp8	sp9	sp10	sp11
T chamber (K)	240	251	241	245	234	232	236	225	236	227	209
ρ chamber (kg/m^3)	73.1	68.3	71.6	70.2	74.4	75.2	73.8	78.7	72.9	77.1	86.7
P chamber (MPa)	5.00	4.93	4.93	4.93	4.94	4.92	4.94	4.95	4.89	4.93	4.96
P chamber (psia)	725	715	715	714	716	714	716	718	709	715	719
T outer (K)	184	176	173	172	175	185	195	183	188	191	150
$\dot{m}$ outer (mg/s)	1170	2800	2780	2810	4550	4240	5750	5810	7050	8140	4620
ρ outer (kg/m^3)	106	113	117	118	115	104	95.7	107	100	99.0	165
u outer (m/s)	4.23	9.46	9.09	9.10	15.2	15.7	23.0	20.9	26.9	31.5	10.7
Re outer	13.5	32.9	32.9	33.3	53.6	48.8	64.6	67.3	80.9	92.5	54.6
T inner (K)	132	137	134	133	137	136	147	138	141	141	132
$\dot{m}$ inner (mg/s)	293	294	291	293	296	295	295	292	293	293	294
ρ inner (kg/m^3)	416	266	342	373	271	302	179	264	214	216	423
u inner (m/s)	3.47	5.45	4.20	3.88	5.38	4.83	8.12	5.45	6.76	6.69	3.42
Re inner	27.5	43.7	34.7	31.7	43.4	39.7	53.4	43.6	49.8	49.4	26.9
VR	1.23	1.75	2.18	2.36	2.85	3.27	2.86	3.86	4.01	4.74	3.15
MR	0.384	1.30	1.63	1.77	3.42	3.66	4.35	6.00	7.55	10.3	3.87
Acoustics Off											
L/d1	13.9	4.91	4.42	5.18	3.25	3.49	1.97	1.96	1.74	1.68	4.03
L_T/d1	16.4	5.12	5.35	5.45	3.46	3.64	2.11	2.17	2.17	2.12	4.08
Acoustics On											
Frequency (kHz)		3.11	3.29	3.26	3.26	3.22	3.08	3.19	3.08	3.05	3.10
L/d1		2.92	2.70	3.58	2.32	2.54	2.05	1.84	1.55	1.45	3.40
L_T/d1		3.18	3.38	3.92	2.65	2.85	2.09	2.12	2.06	2.06	3.45

Acknowledgments

The authors would like to recognize Randy Harvey for his invaluable contributions on running and maintaining the facility. Also thanks to Juan Rodriguez for preparing the appendix. This work is sponsored by AFOSR under Mitat Birkan, program manager.

References

1. Oschwald, M., Smith, J. J., Branam, R., Hussong, J., Schik, A., Chehroudi, B., Talley, D., "Injection of Fluids into Supercritical Environments", Combustion Science and Technology, Vol. 178, No. 1-3, 2006, pp. 49-100.
2. Culick F. E. and Yang, V., "Overview of Combustion Instabilities in Liquid-Propellant Rocket Engines," Liquid Rocket Engine Combustion Instability, edited by V. Yang and W. Anderson, Progress in Astronautics and Aeronautics, AIAA, Washington, DC, 1995, pp. 3-38.
3. Muss, J., Chakroborty, S., Leyva, I. A., "Development of the Scorpius LOX/Kerosene engine family", JANNAF 2005-0356, 2nd Liquid Propulsion and 1st Spacecraft Propulsion Subcommittee Meeting, Monterey, California, December 5-8, 2005.

4. Marshall, W., Pal, S., Woodward, R., Santoro, R. J., Smith, R., Xia, G., Sankaran, V., Merkle, C. L., "Experimental and Computational Investigation of Combustor Acoustics and Instabilities, Part II: Transverse Modes"; AIAA 2006-538
5. Yang., V., Anderson W., editors, "Liquid Rocket Engine Combustion Instability", Progress in Astronautics and Aeronautics, Vol. 169, 1995
6. Sutton, G. P., "Rocket Propulsion Elements", Sixth Edition, John Wiley & Sons, Inc., NY, 1992
7. Davis, D. W., Chehroudi, B., "Measurements in an acoustically driven coaxial jet under sub-, near-, and supercritical conditions", JPP, Vol. 23, No. 2, March- April 2007
8. Davis, D. W., Chehroudi, B., Sorensen, I., "Measurements in an acoustically driven coaxial jet under supercritical conditions", AIAA 2005-736
9. REFPROP, Reference Fluid Thermodynamic and Transport Properties, Software Package, Ver. 7.0, NIST, U.S. Department of Commerce, Gaithersburg, MD, 2002.
10. Otsu, N., "A threshold selection method from gray-level histograms", IEEE transactions on Sytems, Man, and Cybernetics, Vol. 9, No. 1, 1979, pp. 62-66.
11. Davis, D., "On the behavior of a shear-coaxial jet, spanning sub- to supercritical pressures, with and without an externally imposed transverse acoustic field", Ph.D. Thesis, 2005